PAPER

Enhanced photocatalytic water splitting of a SILAR deposited α-Fe$_2$O$_3$ film on TiO$_2$ nanoparticles

Zahra-Sadat Pourbakhsh,[a] Kyana Mohammadi,[a] Ahmad Moshaii, [ID] *[a] Maryam Azimzadehirani[b] and Amir Hosseinmardi[a]

We have investigated the effect of deposition of a α-Fe$_2$O$_3$ thin layer on a substrate of TiO$_2$ nanoparticles for photoelectrochemical (PEC) water splitting. The TiO$_2$ layer was coated on an FTO substrate using the paste of TiO$_2$ nanoparticles. The α-Fe$_2$O$_3$ layer was deposited on the TiO$_2$ thin film, using the method of Successive Ionic Layer Adsorption and Reaction (SILAR) with different cycles. Various characterizations including XRD, EDX and FE-SEM confirm the formation of α-Fe$_2$O$_3$ and TiO$_2$ nanoparticles on the electrode. The UV-visible absorption spectrum confirms a remarkable enhancement of the absorption of the α-Fe$_2$O$_3$/TiO$_2$/FTO composite relative to the bare TiO$_2$/FTO. In addition, the photocurrents of the composite samples are remarkably higher than the bare TiO$_2$/FTO. This is mainly due to the low band gap of α-Fe$_2$O$_3$, which extends the absorption spectrum of the α-Fe$_2$O$_3$/TiO$_2$ composite toward the visible region. In addition, the impedance spectroscopy analysis shows that the recombination rate of the charge carriers in the α-Fe$_2$O$_3$/TiO$_2$ is lower than that for the bare TiO$_2$. The best PEC performance of the α-Fe$_2$O$_3$/TiO$_2$ sample was achieved by the sample of 70 cycles of α-Fe$_2$O$_3$ deposition with about 7.5 times higher photocurrent relative to the bare TiO$_2$.

Introduction

Fossil fuels are currently the main non-renewable energy resource in the world, and have negative effects on the environment like greenhouse gas production and global temperature rise. These unclean fuels cannot meet the continuously increasing future demands for energy resources.[1–4] Hydrogen as a non-polluting fuel can be considered as a good candidate of sustainable energy resources.[5] Of various methods to produce hydrogen, efficient photoelectrochemical (PEC) water splitting provides a promising pathway for solar-to-hydrogen conversion using cost-effective semiconductor materials.[6–9]

In PEC water splitting, hydrogen is generated by the absorption of light in a semiconductor, which must have a suitable bandgap and suitable energies of conduction and valance bands relative to the oxidation and reduction potentials of water. Also, it should be chemically stable in the electrolyte of the PEC process.[10–12]

In recent years, TiO$_2$ nanoparticles have been extensively studied for PEC water splitting due to their low cost, simple preparation, non-toxicity and chemical stability. However, the high bandgap of TiO$_2$ (3.2 eV for the anatase and 3.0 eV for the rutile phase) only allows absorption of the ultraviolet region of

sun light, which covers only 5% of the solar spectrum. This significantly decreases the efficiency of PEC using the TiO$_2$ nanostructures. To improve the PEC properties of TiO$_2$, many methods such as sensitization to the sunlight with doping of nitrogen or heavy metals[13–17] and incorporating plasmonic nanoparticles such as Ag, Au, Pt[18–20] have been investigated in the literatures. Most of these approaches have the drawback of increasing crystal deformations or introducing defects that act as additional electron–hole recombination centers.[21–26] In addition, combining TiO$_2$ with another semiconductor with suitable band alignments has been reported to achieve larger electron/hole separation due to the movement of charge carriers between the different semiconductors. With this regard, Fe$_2$O$_3$ with a bandgap of about 1.9–2.2 eV, which can absorb photons of visible light spectrum,[27,28] is a suitable semiconductor to be mixed with TiO$_2$ to extend the adsorption spectrum of the composite efficiency.[29] However, two main disadvantages of Fe$_2$O$_3$ are the low conductivity and a short diffusion length of excitons (2–20 nm), which significantly diminish its photocatalytic efficiency.[30,31] However, these deficiencies of Fe$_2$O$_3$ can be resolved by combining TiO$_2$ with Fe$_2$O$_3$, due to a strong electric field at the interface of Fe$_2$O$_3$/TiO$_2$.[30–32] Accordingly, the combination of these two semiconductors has attracted many attentions recently.[33–43]

In this work, a composite electrode of α-Fe$_2$O$_3$/TiO$_2$ was introduced as a photoanode for PEC cells. The SILAR method was used for the deposition of α-Fe$_2$O$_3$ on the TiO$_2$ substrate. Fig. 1 shows a schematic of the composite electrode in the

[a]Department of Physics, Tarbiat Modares University, P.O Box 14115-175, Tehran, Iran. E-mail: moshaii@modares.ac.ir

[b]Department of Chemistry, Tarbiat Modares University, P.O Box 14115-175, Tehran, Iran
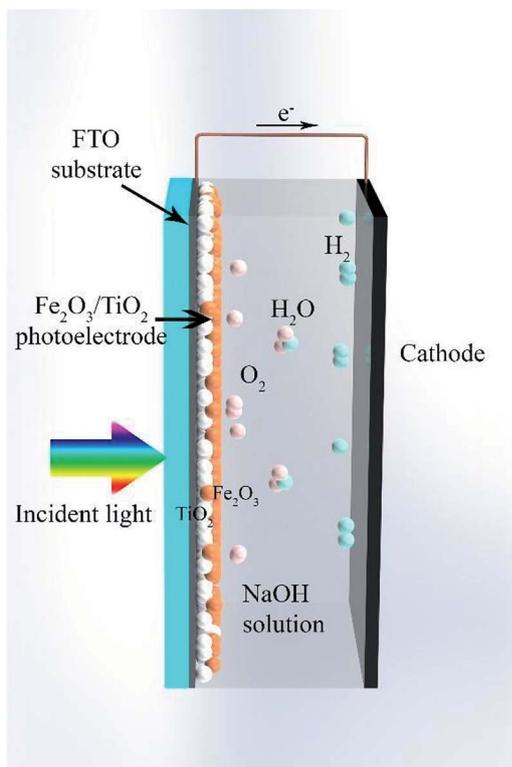
Fig. 1 Schematic of the composite electrode of α-Fe$_2$O$_3$/TiO$_2$ in the water splitting process.

Fig. 2 A schematic of the SILAR process for deposition of α-Fe$_2$O$_3$ nanoparticles on a sample for one cycle.

water-splitting process. Under visible light irradiation, the composite electrode produces electron–hole pairs and the holes oxidize water at the electrode surface to generate oxygen. The produced electrons migrate to the counter electrode and take part in the reduction of water to produce hydrogen. We studied the optimum thickness of α-Fe$_2$O$_3$ on the TiO$_2$ substrate to obtain the best water-splitting activity. We found that under 70-cycle deposition of α-Fe$_2$O$_3$, the best PEC water-splitting activity occurs, which corresponds to about 7.5 times photocurrent improvement relative to the bare TiO$_2$ electrode. This result is mainly due to extension of the absorption spectrum of the sample into the visible light, due to incorporating α-Fe$_2$O$_3$. In addition, the recombination of charge carriers greatly decreases by using the α-Fe$_2$O$_3$/TiO$_2$ composite.

Experimental section

The TiO$_2$ layer was deposited on an area of 1 cm × 1 cm of the FTO substrate (with the sizes of 1 cm × 2 cm) by the doctor blade method,[44] using the paste of TiO$_2$ (Degussa, P-25) purchased from Sharifsolar. Then, a thin film of α-Fe$_2$O$_3$ nanoparticles was deposited on the TiO$_2$ layer by the SILAR method, which provides a strong control over the film thickness. In this method, 0.05 M FeCl$_3$ and 0.1 M NaOH, were used as iron and hydroxide precursors.[42] The synthesis process is shown in Fig. 2, in which each immersion stage lasted 10 seconds. After depositing 30 cycles, the solutions of FeCl$_3$ and NaOH were renewed by the fresh ones. The deposition of Fe$_2$O$_3$
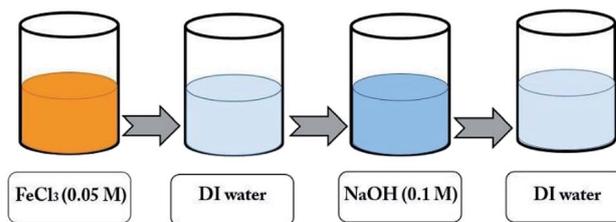
on the samples by the SILAR method was done with various cycles of 50, 60, 70 and 80th. After finishing the SILAR deposition, we completely remove the tiny layer of α-Fe$_2$O$_3$ on the back of FTO by ethanol. Then the composite samples were placed inside a furnace for annealing at 550 °C for 4 hours. Fig. 3 shows a photo of the samples fabricated by the SILAR method with different cycles.

For the electrochemical measurements, the entire substrate was illuminated by a 100 W Xe lamp, so the illumination area of the α-Fe$_2$O$_3$/TiO$_2$ layer was 1 cm × 1 cm. In addition, the illumination was frontside.

Results and discussion

Characterization

The X-ray diffraction pattern of a sample of α-Fe$_2$O$_3$/TiO$_2$/FTO prepared with 70 SILAR cycles is shown in Fig. 4, using an X-ray diffractometer (Xpert, Philips) with Cu Kα radiation ($\lambda = 1.54$ Å). According to the reference cards of (JCPD-01-083-2243) and (JCPD-01-073-2224), the peaks of the crystalline phases of anatase and rutile of TiO$_2$ are clearly seen at the 2θ angles of 29.5°, 44.2°, 56.4°, 63.5°, 74.4°, 31.9°, 77.8° relating to the planes of (101), (004), (200), (105), (204), (110), and (221), respectively. The substrate peaks of SnO$_2$ are identified, in the pattern, according to the card of (JCPD-01-077-0450). On the other hand, the diffraction peaks of α-Fe$_2$O$_3$ nanoparticles are characterized at the angles of 38.8°, 41.7°, 47.9°, 58.2° and 74.1°, relating to the planes of (104), (110), (113), (024), (116) and (214), according to the card of (JCPD-01-086-0550).
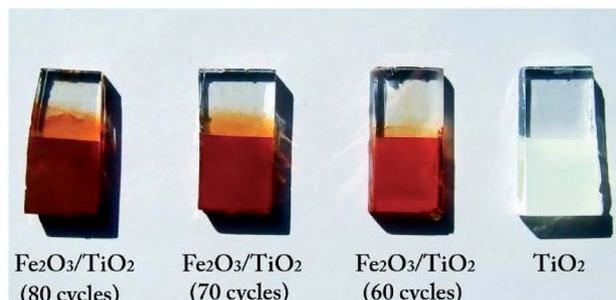

Fig. 3 A photograph of the samples of α-Fe$_2$O$_3$/TiO$_2$/FTO with different SILAR deposition cycles of α-Fe$_2$O$_3$.
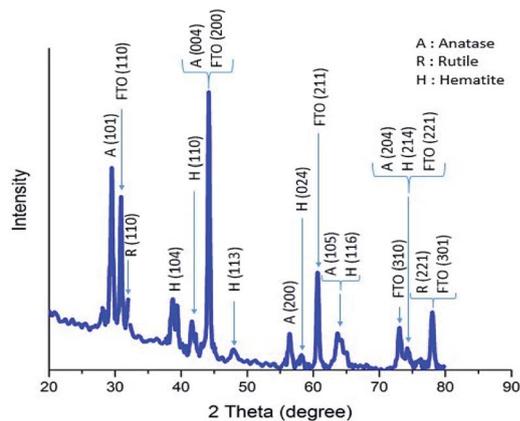
Fig. 4 XRD diffraction pattern of a sample of α-Fe_2O_3/TiO_2/FTO prepared with 70 SILAR cycles.

In order to investigate the morphology of the samples, the Field Emission Scanning Electron Microscopy (FESEM) of the samples was taken using the MIRA3 TESCAN microscope. The top and the cross-section images of the TiO_2 samples are shown in Fig. 5. We see that the thickness of the TiO_2 layer on the surface is around 400 nm. While a very thick layer of Fe_2O_3 (about 18 μm) is produced on the sample by the 70-cycle SILAR deposition.

The EDX analysis was used for elemental determination of the samples. The weight percentages of the elements Ti, O, Fe and Au (which is used for preparation of the layers for EDX/
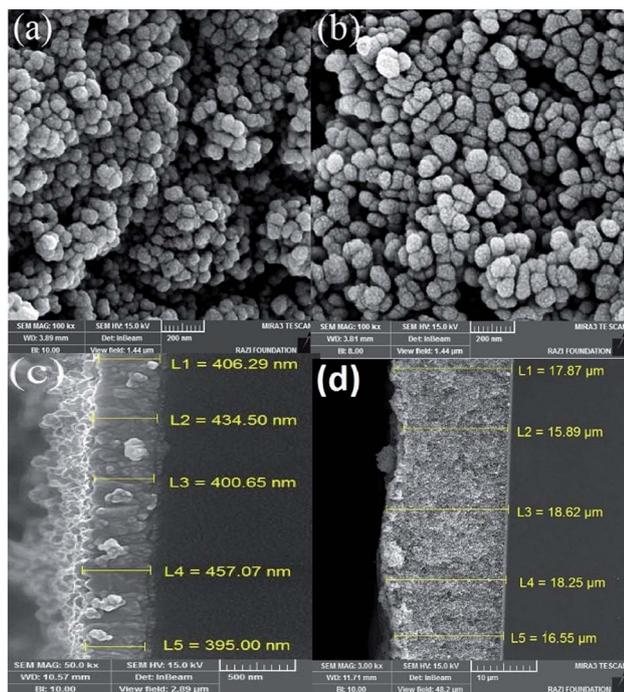
Fig. 5 FE-SEM images from various samples of (a) TiO_2/FTO, (b) α-Fe_2O_3/TiO_2/FTO with 70 SILAR cycles, (c) cross-sectional image of TiO_2/FTO, (d) cross-sectional image of α-Fe_2O_3/TiO_2/FTO with 70 SILAR cycles.
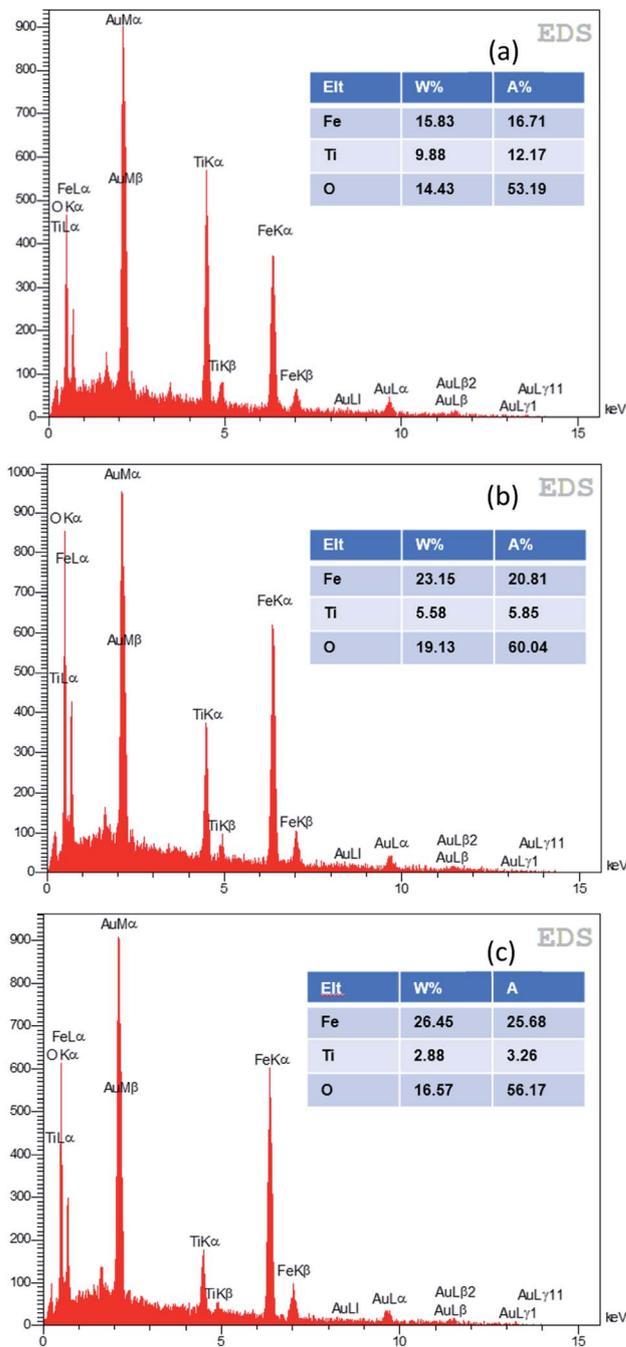
Fig. 6 EDX analysis of various samples of α-Fe_2O_3/TiO_2/FTO with (a) 60, (b) 70, (c) 80 SILAR cycles.

FESEM) for the samples with different SILAR cycles are shown in Fig. 6. It is seen that the iron percentage of the best α-Fe_2O_3/ TiO_2 sample for the PEC application (which is the 70-cycle sample) was about 23.15% (wt).

Fig. 7 shows the UV-vis absorption spectrums of the bare TiO_2 and the α-Fe_2O_3/TiO_2 sample with the 70-cycle. The bare TiO_2 has an absorption edge around 390 nm ($\sim$3.13 eV), which is related to its wide bandgap. The absorption edge of α-Fe_2O_3/ TiO_2 has been transferred to the visible range with a much
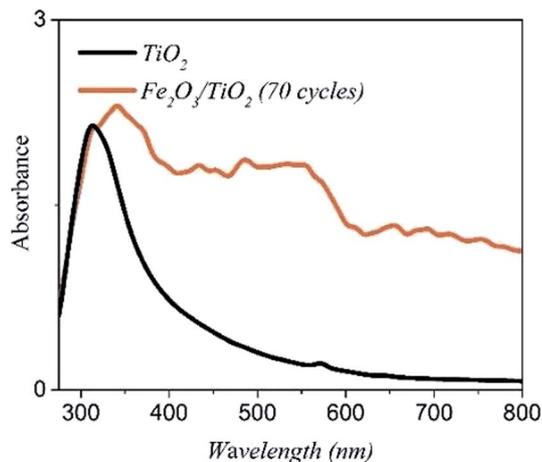
Fig. 7 The UV-vis spectra of the samples of TiO_2/FTO and α-Fe_2O_3/TiO_2/FTO with 70-cycle.

higher absorption intensity than the bare TiO_2 in the range of 400–800 nm.

The bandgaps of the fabricate TiO_2 and Fe_2O_3/TiO_2 film are calculated using the Tauc plot. As it showed in Fig. 8, the tangent lines indicates that the Fe_2O_3 has an indirect band gap of about 2.04 eV and direct band gap of TiO_2 is about 3.35 eV for our sample; which is agreed with other observations.[42,45]

Photoelectrochemical characterization

Fig. 9 shows the results of PEC measurements for the α-Fe_2O_3/ TiO_2 samples. The photoelectrochemical properties were
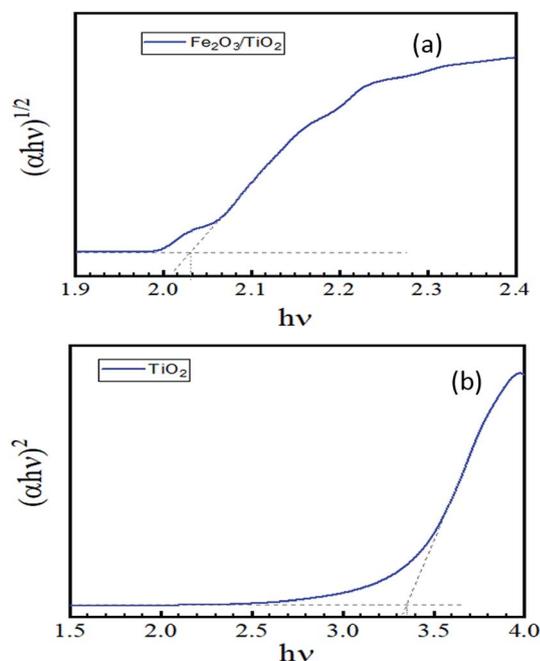

Fig. 8 Tauc plot calculated to find the band gap of the layer from the UV-vis spectrum (a) α-Fe_2O_3/TiO_2 (b) pure TiO_2.

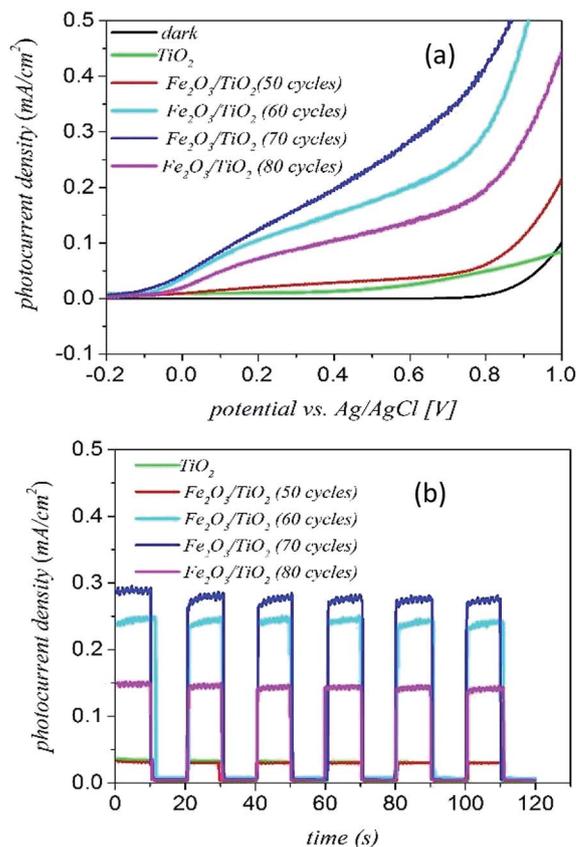Fig. 9 (a) The J–V measurement curves and (b) chronoamperometry measurements of the α-Fe_2O_3 loaded TiO_2/FTO samples with different deposition cycles.

carried out using a three-electrode cell with the sample as the working electrode, a Pt wire as the counter electrode and the Ag/ AgCl electrode saturated with 3 M KCl as the reference electrode. The electrolyte was 1 M NaOH solution.

Fig. 9(a) shows the photocurrent–voltage (J–V) curves of various samples for both dark and light illuminations. The dark current curves of all samples are close to zero with no photoelectrochemical activity under the dark condition. The bare sample of TiO_2 has a small photocurrent density of around 0.04 mA cm^{-2}. The J–V curves of the samples confirm that the current density of the 70 cycles deposition of α-Fe_2O_3 gives the highest photocurrent (around 0.3 mA cm^{-2}). With increasing the number of deposition cycles to 80 cycles, the current density of the sample decreases. In fact, the 70-cycle deposition of α-Fe_2O_3 is the optimum thickness for getting the best water-splitting properties from the composite sample.

Fig. 9(b) shows the transient photocurrent curves of various samples for the ON–OFF period of 20 s. We see that the photocurrent rapidly increases when the light is turned on and it immediately decreased to zero when the light is turned off. According to the results of Fig. 9(b), after about 80 seconds, the photocurrent becomes stable and repeatable. In addition, there is a small slope for the current curve under the light ON

condition indicating that the electron–hole recombination is small in the complex of α-Fe_2O_3/TiO_2/FTO.

The main reason for increment of the photocurrent density of the α-Fe_2O_3/TiO_2/FTO electrode relative to the bare TiO_2 goes back to the higher absorption of the composite material. As shown in Fig. 7, TiO_2 mainly absorb short wavelength photons below 400 nm. However, adding α-Fe_2O_3 to the electrode can extend the optical absorption to the visible spectrum.[46] As a result, the low energy photons can be absorbed by the α-Fe_2O_3 part of the photoelectrode and more photoelectrons can be produced by the composite electrode.[47]

The next reason is the location of the α-Fe_2O_3 edge conduction band compare to TiO_2 (as shown in Fig. 10). Under UV-vis illumination, electrons can be excited from the valence band (VB) to the conduction band (CB) of the anatase, creating a charge vacancy in the VB. In the absence of the α-Fe_2O_3, most of electron–holes are combined quickly.[39,47]

Increasing the coating cycles of hematite (from 50 to 70 cycles), had a significant improvement in current density. According to the results of Fig. 9, the sample of 70-cycle represents the best photocurrent. However, with increasing the number of cycles to 80 cycles, the photocurrent density decreases. Therefore, it is indicated that there was an optimal amount of deposition layer. By increasing the amount of α-Fe_2O_3 nanoparticles on the surface of the TiO_2 nanoparticles, the surface was blocked and light access was greatly reduced, and the production of the electron–hole decreased, so the photocurrent was reduced. So when the amount of α-Fe_2O_3 was increased from an optimal amount, because photoelectrons accumulated on α-Fe_2O_3, the recombination probability of the electron–holes increased.[48] So α-Fe_2O_3 being as an electron–hole recombination center, and resulted a reduction in optical activity.[49]

In order to investigate the charge transport properties of the bare TiO_2 and α-Fe_2O_3/TiO_2 samples, the electrical impedance spectroscopy measurements (EIS) were performed for various samples. The applied frequency range was from 100 mHz to 100 kHz (in a 0.1 M Na_2SO_4 electrolyte at the potential of $V = 0.7$ V versus the Ag/AgCl reference). The Nyquist plots obtained by the EIS measurements in addition to the equivalent RC circuit for
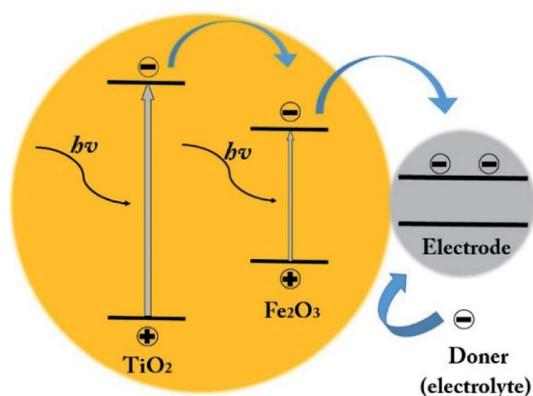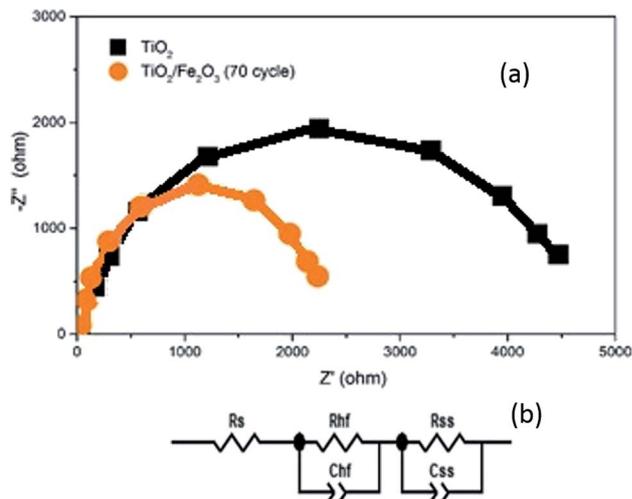

Fig. 11 (a) Nyquist plots of TiO_2/FTO and the sample of α-Fe_2O_3/TiO_2/FTO with 70 cycles. (b) The equivalent circuit used for the fitting of EIS results.

fitting the EIS data are shown in Fig. 11. In the equivalent circuit, R_s indicates a serial resistance between the FTO substrate and the TiO_2 layer. R_{hf} demonstrates the high frequency resistance due to accumulation and trapping of fast charges throughout the α-Fe_2O_3/TiO_2 composite. R_{ss} represents the resistance of charge transfer between the photoanode and the electrolyte. The capacitances C_{hf} and C_{ss} are relating to the space charge capacitance of the sample and the capacitance associated with the surface states of the photoanode, respectively.

As shown in Fig. 11, the curve of α-Fe_2O_3/TiO_2 photoanode has a smaller semicircle radius than the bare TiO_2, which indicates that both R_{hf} and R_{ss} are lower for the α-Fe_2O_3/TiO_2 relative to the bare TiO_2. This result completely confirms the improvement of charge transfer kinetics of the bare TiO_2 sample after the Fe_2O_3 modification. The faster charge transfer of the 70-cycle sample leads to less surface recombination and improving the photocatalytic activity of this sample relative to all other ones.

It should be mentioned that TiO_2 has better charge transport properties relative to Fe_2O_3, considering the mobility of electrons and the holes in both semiconductors. Therefore, deposition of a thin layer of TiO_2 under Fe_2O_3 in the samples causes that the electrons are better transmitted to the external circuit relative to the case of blank Fe_2O_3 on FTO. In fact, the recombination between electron and holes at the interface of TiO_2/FTO is less than that of Fe_2O_3/FTO. Consequently, a higher photocurrent is expected from the stack of Fe_2O_3/TiO_2/FTO relative to that of Fe_2O_3/FTO. This issue has clearly been confirmed by other researchers.[42]

Conclusions

In this work, we reported on the effect of deposition of a thin layer of α-Fe_2O_3 on TiO_2 nanoparticles by the SILAR method for

Fig. 10 Schematic of the electron–hole generation and the transferring of the photogenerated charges into the photoanode under the visible light illumination.

photoelectrochemical water splitting. The formation of α-Fe$_2$O$_3$ was confirmed by various characterizations including XRD, EDX and FE-SEM spectroscopy. The UV-visible absorption spectrum showed a remarkable enhancement in the absorption of α-Fe$_2$O$_3$/TiO$_2$ relative to the bare TiO$_2$. The photoelectrochemical characterizations indicate that all samples of α-Fe$_2$O$_3$/TiO$_2$ have an improved photocurrent compared to the bare TiO$_2$. This result is mainly due to the proper bandgap of α-Fe$_2$O$_3$, which extended the absorption spectrum of the sample into the visible light. Also, the recombination of charge carriers greatly decreased by using α-Fe$_2$O$_3$ on TiO$_2$. We found that there is an optimum number of cycles for the SILAR deposition of α-Fe$_2$O$_3$, on TiO$_2$, which is the 70-cycle exhibiting much better photoelectrochemical activity from α-Fe$_2$O$_3$/TiO$_2$ relative to the bare TiO$_2$, with about 7.5 times photocurrent improvement.

Conflicts of interest

There are no conflicts to declare.

Acknowledgements

References

1 K. Feron, W. J. Belcher, C. J. Fell and P. C. Dastoor, *Int. J. Mol. Sci.*, 2012, **13**, 17019–17047.

2 M. K. Nazeeruddin, E. Baranoff and M. Grätzel, *Sol. Energy*, 2011, **85**, 1172–1178.

3 F. E. Osterloh and B. A. Parkinson, *MRS Bull.*, 2011, **36**, 17–22.

4 N. S. Lewis and D. G. Nocera, *Proc. Natl. Acad. Sci. U. S. A.*, 2006, **103**, 15729–15735.

5 N. S. Lewis, *Science*, 2013, **798**, 798–802.

6 T. Hisatomi, J. Kubota and K. Domen, *Chem. Soc. Rev.*, 2014, **43**, 7520–7535.

7 A. Kudo and Y. Miseki, *Chem. Soc. Rev.*, 2009, **38**, 253–278.

8 J. Schneider, H. Jia, J. T. Muckerman and E. Fujita, *Chem. Soc. Rev.*, 2012, **41**, 2036.

9 X. Huang, S. Han, W. Huang and X. Liu, *Chem. Soc. Rev.*, 2013, **42**, 173–201.

10 M. R. Hoffmann, S. Martin, W. Choi and D. W. Bahnemann, *Chem. Rev.*, 1995, **95**, 69–96.

11 A. L. Linsebigler, A. L. Linsebigler, J. T. Yates Jr, G. Lu, G. Lu and J. T. Yates, *Chem. Rev.*, 1995, **95**, 735–758.

12 J. Li and N. Wu, *Catal. Sci. Technol.*, 2015, **5**, 1360–1384.

13 N. Lu, X. Quan, J. Li, S. Chen, H. Yu and G. Chen, *J. Phys. Chem. C*, 2007, **111**, 11836–11842.

14 J. H. Park, S. Kim and A. J. Bard, *Nano Lett.*, 2006, **6**, 24–28.

15 Y. Huo, Y. Jin, J. Zhu and H. Li, *Appl. Catal., B*, 2009, **89**, 543–550.

16 L. Sun, J. Li, C. L. Wang, S. F. Li, H. B. Chen and C. J. Lin, *Sol. Energy Mater. Sol. Cells*, 2009, **93**, 1875–1880.

17 H. Liu, G. Liu and Q. Zhou, *J. Solid State Chem.*, 2009, **182**, 3238–3242.

18 H.-J. Lin, T.-S. Yang, C.-S. Hsi, M.-C. Wang and K.-C. Lee, *Ceram. Int.*, 2014, **40**, 10633–10640.

19 Y.-H. Lin, T.-K. Tseng and H. Chu, *Appl. Catal., A*, 2014, **469**, 221–228.

20 S. Lin, D. Li, J. Wu, X. Li and S. A. Akbar, *Sens. Actuators, B*, 2011, **156**, 505–509.

21 J. S. Im, S. K. Lee and Y. S. Lee, *Appl. Surf. Sci.*, 2011, **257**, 2164–2169.

22 M. H. H. Mahmoud, A. A. Ismail and M. M. S. Sanad, *Chem. Eng. J.*, 2012, **187**, 96–103.

23 S. Zhan, J. Yang, Y. Liu, N. Wang, J. Dai, H. Yu, X. Gao and Y. Li, *J. Colloid Interface Sci.*, 2011, **355**, 328–333.

24 B. Liu, H. M. Chen, C. Liu, S. C. Andrews, C. Hahn and P. Yang, *J. Am. Chem. Soc.*, 2013, **135**, 9995–9998.

25 T. K. Ghorai, M. Chakraborty and P. Pramanik, *J. Alloys Compd.*, 2011, **509**, 8158–8164.

26 Y. C. Pu, G. Wang, K. Der Chang, Y. Ling, Y. K. Lin, B. C. Fitzmorris, C. M. Liu, X. Lu, Y. Tong, J. Z. Zhang, Y. J. Hsu and Y. Li, *Nano Lett.*, 2013, **13**, 3817–3823.

27 M. Mishra and D.-M. Chun, *Appl. Catal., A*, 2015, **498**, 126–141.

28 K. M. H. Young, B. M. Klahr, O. Zandi and T. W. Hamann, *Catal. Sci. Technol.*, 2013, **3**, 1660.

29 A. B. Murphy, P. R. F. Barnes, L. K. Randeniya, I. C. Plumb, I. E. Grey, M. D. Horne and J. A. Glasscock, *Int. J. Hydrogen Energy*, 2006, **31**, 1999–2017.

30 T. Hisatomi, H. Dotan, M. Stefik, K. Sivula, A. Rothschild, M. Grätzel and N. Mathews, *Adv. Mater.*, 2012, **24**, 2699–2702.

31 P. Liao and E. A. Carter, *J. Appl. Phys.*, 2012, **112**, 1775–1781.

32 V. N. Nguyen, N. K. T. Nguyen and P. H. Nguyen, *Adv. Nat. Sci.: Nanosci. Nanotechnol.*, 2011, **2**, 035014.

33 W.-H. Hung, T.-M. Chien and C.-M. Tseng, *J. Phys. Chem. C*, 2014, **118**, 12676–12681.

34 N. A. M. Barakat, A. Taha, M. Motlak, M. M. Nassar, M. S. Mahmoud, S. S. Al-Deyab, M. El-Newehy and H. Y. Kim, *Appl. Catal., A*, 2014, **481**, 19–26.

35 T. Wang, G. Yang, J. Liu, B. Yang, S. Ding, Z. Yan and T. Xiao, *Appl. Surf. Sci.*, 2014, **311**, 314–323.

36 M. A. Mahadik, S. S. Shinde, V. S. Mohite, S. S. Kumbhar, A. V. Moholkar, K. Y. Rajpure, V. Ganesan, J. Nayak, S. R. Barman and C. H. Bhosale, *J. Photochem. Photobiol., B*, 2014, **133**, 90–98.

37 B. Kiliç, N. Gedik, S. P. Mucur, A. S. Hergul and E. Gür, *Mater. Sci. Semicond. Process.*, 2015, **31**, 363–371.

38 S. Zhu, F. Yao, C. Yin, Y. Li, W. Peng, J. Ma and D. Zhang, *Microporous Mesoporous Mater.*, 2014, **190**, 10–16.

39 X. Zhang, Y. Xie, H. Chen, J. Guo, A. Meng and C. Li, *Appl. Surf. Sci.*, 2014, **317**, 43–48.

40 N. Sobti, A. Bensouici, F. Coloma, C. Untiedt and S. Achour, *J. Nanopart. Res.*, 2014, **16**, 2577.

41 P. Luan, M. Xie, D. Liu, X. Fu and L. Jing, *Sci. Rep.*, 2015, **4**, 6180.

42 A. J. Abel, I. Garcia-Torregrosa, A. M. Patel, B. Opasanont and J. B. Baxter, *J. Phys. Chem. C*, 2015, **119**, 4454–4465.

43 W. Jo and N. C. S. Selvam, *Dalton Trans.*, 2015, **44**, 16024–16035.

44 S. Ito, T. N. Murakami, P. Comte, P. Liska, C. Grätzel, M. K. Nazeeruddin and M. Grätzel, *Thin Solid Films*, 2008, **516**, 4613–4619.

45 B. Eftekharinia, A. Moshaii, A. Dabirian and N. S. Vayghan, *J. Mater. Chem. A*, 2017, **5**, 3412–3424.

46 Y. Xia and L. Yin, *Phys. Chem. Chem. Phys.*, 2013, **15**, 18627–18634.

47 H. Zhao, W. Fu, H. Yang, Y. Xu, W. Zhao, Y. Zhang, H. Chen, Q. Jing, X. Qi, J. Cao, X. Zhou and Y. Li, *Appl. Surf. Sci.*, 2011, **257**, 8778–8783.

48 B. Kim, H. Oh, K. Yun, S. Jung, W. Kang and S. Kim, *Prog. Org. Coat.*, 2013, **76**, 1869–1873.

49 L. Peng, T. Xie, Y. Lu, H. Fan and D. Wang, *Phys. Chem. Chem. Phys.*, 2010, **12**, 8033–8041.